Brodogradnja Volume 77 Number 3 (2026) 77303

University of Zagreb
Faculty of Mechanical
Engineering and Naval
Architecture

journal homepage: www.brodogradnja.fsb.hr

Brodogradnja

An International Journal of Naval Architecture and
Ocean Engineering for Research and Development

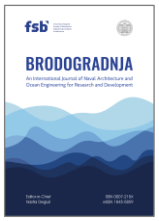

A novel IMGS-GMRES algorithm for addressing ill-conditioned high-dimensional matrices in hydrodynamic analysis of large floating structures

Yiwen Zhang[1,*], *Yonghe Xie*[1], *Wei Wang*[1,2], *Xiwu Gong*[1], *Zhinuo Zhuang*[1]

[1] *School of Naval Architecture and Maritime, Zhejiang Ocean University, Zhoushan 316022, China*
[2] *School of Marine Science and Technology, Northwestern Polytechnical University, Xi'an, China*

ARTICLE INFO

Keywords:
IMGS-GMRES algorithm
Ill-conditioning
Hydrodynamic analysis
Boundary element method
Computational fluid dynamics

ABSTRACT

In large-scale hydrodynamic analyses of large floating structures, conventional iterative algorithms frequently encounter ill-conditioning when solving linear systems derived from boundary element discretisation, typically manifesting as significantly degraded convergence rates or numerical instabilities. To address this challenge, we propose a novel Improved Modified Gram-Schmidt GMRES (IMGS-GMRES) algorithm. This algorithm significantly improves the efficiency and numerical stability in solving ill-conditioned systems by optimising the orthogonalisation process and incorporating preconditioning techniques. The method combines preconditioning strategies with an enhanced Gram-Schmidt orthogonalisation technique to effectively mitigate high condition numbers. The IMGS-GMRES algorithm has been implemented within the in-house hydrodynamic solver FHLAN and validated against the commercial software WADAM, demonstrating improvements in computational accuracy and stability. Furthermore, it optimises the solution process for large-scale linear systems encountered in hydrodynamic analysis. Numerical experiments demonstrate superior performance: for a system with a condition number of 1.06×10^{22}, IMGS-GMRES reduces iterations by 44.8 % (from 498 to 275) and suppresses orthogonality error to the machine precision of 4.11×10^{-16}. In a large-scale case with 31,000 panels, it achieves 82 % runtime reduction vs direct solvers. The algorithm provides an efficient, robust solution for ill-conditioned hydrodynamic analyses of large floating bodies and high-dimensional coupled systems, supporting real-time simulation and optimisation.

1. Introduction

When employing the Boundary Element Method (BEM) for the hydrodynamic analysis of large floating bodies, practical engineering problems often involve complex discretisations with hundreds of thousands to millions of degrees of freedom, leading to severely ill-conditioned linear systems that cause the efficiency of conventional direct solvers to deteriorate sharply as the system size increases [1]. In parallel, concerning the cooperative control of multiple unmanned surface vehicles (MMVs), existing studies have incorporated reinforcement learning (RL) into discrete-time multi-agent systems (MAS) while explicitly accounting for

* Corresponding author.
E-mail address: zhangyiwen202511@163.com

https://doi.org/10.21278/brod77303
Received 14 June 2025; Received in revised form 5 November 2025; Accepted 19 November 2025
Available online 9 December 2025
ISSN 0007-215X; eISSN 1845-5859

actuator faults. By employing critic-actor neural networks to estimate utility functions and uncertain dynamics, these approaches ensure semi-globally uniformly ultimately bounded (SGUUB) closed-loop signals in the Lyapunov sense, and the effectiveness of the proposed strategies has been validated through MMV simulations. Such discrete-time non-strict-feedback MAS controllers, operating under SGUUB guarantees, rely directly on the stability and throughput of underlying linear algebra modules, thereby further underscoring the urgent need for efficient and numerically robust solution kernels [2]. Moreover, the hydrodynamic characteristics of large floating structures are jointly influenced by free-surface effects, complex three-dimensional geometries, and strongly coupled loads. The fluid-structure interaction (FSI) mechanisms further amplify the condition number and ill-posedness of the coefficient matrix, thereby imposing stricter requirements on solution stability and accuracy [3].

As marine structures evolve towards larger scales, the resulting coefficient matrices after discretisation often exhibit extreme ill-conditioning. Efficient matrix-solving methods not only significantly shorten design cycles and reduce computational costs but also meet the demands of real-time simulation and optimisation design. To this end, researchers have generally turned to iterative solution strategies to enhance scalability while ensuring accuracy. In recent years, scholars both domestically and internationally have conducted extensive research on iterative solution methods for the linear systems generated by the Boundary Element Method. Among them, the Generalised Minimal Residual (GMRES) method [4] is considered an effective algorithm for solving dense, asymmetric linear systems. To ensure the linear independence of the Krylov subspace basis vectors, GMRES requires orthogonalisation at each iteration. However, under high-condition-number matrices, the rounding errors of the one-shot CGS/MGS process are repeatedly amplified, leading to the degradation of the basis vector orthogonality and resulting in residual stagnation and oscillation. This mechanism has been confirmed through theoretical analyses of the GMRES behaviour in BEM equations and low-rank and small-norm perturbations ($\boldsymbol{I}$+$\boldsymbol{K}$+$\boldsymbol{E}$) [5, 6]. Therefore, to meet the demands of high-precision hydrodynamic computations for large floating bodies, more robust and efficient orthogonalisation strategies are urgently required.

Hydroelastic analysis of large floating bodies often employs time-domain direct methods and hybrid FEM-BEM frameworks, a process that requires frequent evaluation of free-surface Green's functions and their derivatives, as well as interpolation/tabulation. This procedure is highly sensitive to CPU and memory usage under real sea conditions and external load coupling, and due to geometric singularities and strong coupling, it induces severe ill-conditioning, posing challenges for linear algebraic solvers [7]. Hess and Smith [8] pioneered the construction of a potential flow computation system using direct methods such as Gaussian elimination and LU decomposition. By constructing Green's function integrals on the boundary and performing numerical integration, they transformed the continuous problem into a system of linear algebraic equations. However, such discrete systems are large-scale and densely populated, and practical solutions often rely on iterative methods. For such problems, GMRES, compared to direct methods, primarily uses MatVec operations, offers better scalability, and can be combined with termination criteria based on backward error. However, in high-dimensional ill-conditioned systems, the orthogonalisation process is prone to degradation of Krylov basis orthogonality due to the accumulation of rounding errors, which remains a key cause of slow convergence and loss of accuracy. The GMRES algorithm proposed by Saad and Schultz [9] marked a revolutionary breakthrough in iterative methods, reducing the computational complexity to $O(N^2)$. In early experiments, the GMRES algorithm was based on the classical Arnoldi iteration and employed standard Gram-Schmidt (CGS) orthogonalisation. However, in high-dimensional or ill-conditioned problems, this orthogonalisation method is prone to severe degradation of orthogonality due to the accumulation of rounding errors. Liu [10] proposed a strategy of low-synchronisation Krylov with double orthogonalisation, derived from the trade-off between communication cost and numerical orthogonality, directly inspiring the adoption of dual orthogonalisation to balance stability and efficiency on large-scale platforms. Overall, the evolution of orthogonalisation techniques has consistently focused on enhancing numerical stability and computational efficiency as its core objective. For sparse systems, although reduced precision yields speed benefits, underflow/denormal numbers may trigger instability, necessitating the use of triple-precision iterative refinement and mixed-precision sparse approximate inverse preconditioners [11-13]. At the same time, block Schur, flexible GMRES, and block Kaczmarz have advantages in spectral arrangement and throughput [14],

but the quality of outer orthogonality remains the determining factor for convergence limits. Carson and Higham [15] developed a triple-precision hybrid computational framework, incorporating GMRES preconditioning and dynamic error compensation, which relaxed the condition number limit to $\kappa_\infty(A) \leq 10^8$, but it does not guarantee rapid convergence of GMRES. Carr and De Sturler [5], combining pseudospectral analysis and perturbation theory, pointed out that although spectral clustering away from the origin typically indicates rapid convergence of GMRES, the convergence speed may still significantly slow down when some eigenvalues have poor conditioning. Carson and Lund [16] proposed an improved block Gram-Schmidt algorithm, incorporating Pythagorean correction, low-synchronisation design, and mixed precision, which guarantees accuracy and improves the efficiency of linear system solvers. Sun and Zheng [6] proposed a BS preconditioner designed for slender beam geometries, combined with modified Gram-Schmidt and Householder transformations, which significantly enhanced the numerical stability of GMRES solvers for BEM equations in thin-walled structures, with iteration efficiency improving by more than three times. Zhou et al. [17] proposed an improved block triangular splitting preconditioner, which significantly reduced the condition number through matrix decomposition and was successfully applied to the solution of three-dimensional linearised Navier-Stokes equations. Simoncini et al. [18] proposed an adaptive block GMRES method designed for multiple right-hand side problems (such as uncertainty quantification), which effectively reduces redundant computations and improves efficiency through block orthogonalisation. In real-time control scenarios such as robust control of multi-agent systems (including actuator faults), both efficiency and numerical stability are equally crucial; a fast and stable linear solver directly impacts online control laws and fault tolerance performance [19], thus the proposed method in this paper has potential transferability. Furthermore, for discrete-time non-strict feedback MAS, Bai and Zhang et al. [20] avoided the non-causal issue of backstepping through system transformations and reduced complexity, employing dynamic compensation + neural networks to eliminate algebraic loops, and constructed an MGR-RL optimal controller to achieve SGUUB; together with [2], this demonstrates the real demand for a stable and efficient solving kernel in the control layer's forward pull.

Although previous work has made progress in the orthogonalisation stability and efficiency of GMRES, in high-condition-number marine engineering BEM problems [21], the one-shot MGS/CGS orthogonalisation process remains susceptible to loss of orthogonality due to the accumulation of rounding errors, leading to residual stagnation or oscillation. This phenomenon has been reported in theoretical analyses and BEM scenarios [5, 6]. Moreover, how to decouple and synergise robust orthogonalisation with structured preconditioners (such as block triangular, Schur), mixed precision, and block Krylov strategies to balance both stability and throughput, remains lacking in systematic engineering-level validation [13, 14, 18]. Finally, the integrated "efficiency-stability" framework for multiple operating conditions, multiple right-hand sides, and large-scale grids remains insufficient, making it difficult to maintain the overall efficiency required for industrial cases while ensuring numerical robustness.

Building on the aforementioned background and theory, this paper proposes an improved double orthogonalisation Generalised Minimal Residual algorithm (IMGS-GMRES), which introduces double (second) orthogonalisation and residual compensation into the GMRES and Arnoldi processes. This reduces the orthogonality error of the basis vectors from $O(u)$ to $O(u^2)$, ensuring monotonic convergence and improving efficiency in high-dimensional, ill-conditioned scenarios. The core contributions of this study can be summarised in the following four aspects:

(1) An IMGS strategy based on a double orthogonalisation mechanism is proposed: building upon the traditional MGS single projection, a second orthogonalisation operation is introduced to compensate for and correct the residual errors after the first orthogonalisation. This design systematically reduces the orthogonality error of the Krylov subspace basis vectors from $O(u)$ to $O(u^2)$, significantly enhancing the numerical robustness of the algorithm in extremely ill-conditioned problems.

(2) A complete IMGS-GMRES algorithm framework integrating preprocessing techniques is constructed: IMGS is decoupled and integrated with structured preconditioners such as block triangular splitting and Schur, inheriting the advantages of spectral clustering and reduced iteration counts without sacrificing stability [17].

(3) Engineering validation was completed in the self-developed FHLAN: compared to WADAM, it maintains consistent engineering accuracy, significantly reducing the total computation time in large-scale grids relative to direct methods, and reducing iteration and reorthogonalisation overhead relative to one-shot MGS-GMRES (see Section 3). Furthermore, as the number of grid elements increases from the thousand-level to the ten-thousand-level, the iteration count of IMGS-GMRES decreases continuously relative to MGS, and compared to direct methods, the total computation time shows a trend of "greater acceleration with larger scale", demonstrating the clear efficiency gains of this method in engineering-scale ship hydrodynamic cases.

(4) Selection recommendations: In medium to large-scale grids (tens of thousands of elements) and in more significantly ill-conditioned scenarios, IMGS-GMRES demonstrates superior overall runtime and convergence performance compared to direct methods and one-shot MGS-GMRES; however, for small-scale problems, direct methods still have a constant term advantage (see Section 3 for empirical results).

The subsequent sections of this paper are organised as follows: Section 2 will provide a detailed introduction to the theoretical model of the IMGS-GMRES algorithm and outline the specific computational process. The algorithm will be successfully embedded in the self-developed hydrodynamic solver FHLAN, and a complete hydrodynamic analysis workflow will be established. Section 3 will present numerical test results, including a comparison of computational accuracy with the commercial software WADAM, a comparison of orthogonalisation performance with the MGS algorithm, and a comparison of computational efficiency with traditional direct solvers. Section 4 will summarise the findings of this paper and discuss the applicability of the IMGS-GMRES algorithm in practical engineering.

2. Theoretical model

To systematically address convergence stability issues in ill-conditioned BEM linear systems for hydrodynamic analysis, this study builds upon an in-depth analysis of the pathogenesis of matrix ill-conditioning and introduces an enhanced dual-orthogonalisation strategy. This strategy is integrated within the GMRES iterative framework, forming the IMGS-GMRES algorithm.

By enhancing the orthogonality of the Krylov subspace basis vectors, this approach effectively mitigates residual stagnation and iterative instability exhibited by conventional MGS methods in high-dimensional, strongly coupled systems. Beginning with the theoretical foundations of the algorithm, this section elaborates the mathematical basis and implementation workflow of the IMGS-GMRES methodology. It provides a detailed analysis of its core mechanisms for addressing problems characterised by high condition numbers, specifically through integration with Arnoldi iteration and preconditioning strategies. This establishes the theoretical foundation for its subsequent integration and application within the FHLAN programme.

2.1 IMGS-GMRES theoretical framework

Linear systems arising from the discretisation of BEM are typically severely ill-conditioned [22, 23], with condition numbers often exhibiting condition numbers in the range of 10^8 to 10^{12}. This ill-conditioning primarily arises from three sources: (1) Singular or near-singular integrals in boundary integral equations introduce substantial magnitude discrepancies among matrix elements during discretisation; (2) The coefficient matrix is typically dense, limiting the effectiveness of conventional preconditioning techniques; (3) Numerical singularities arising from free surface effects or geometric singularities further exacerbate matrix ill-conditioning [24].

These factors collectively lead to stagnation or oscillation in residual convergence when the conventional GMRES method is used with a single MGS orthogonalisation strategy. To address this challenge, this study proposes IMGS orthogonalisation strategy to significantly enhance the numerical stability of the GMRES algorithm when solving ill-conditioned matrices.

The core improvement of the method lies in the incorporation of a dual orthogonalisation strategy within the Arnoldi process. Specifically, after performing a single MGS orthogonalisation on the double-precision floating-point vector ω, the theoretical residual $\|\delta_1\|$ satisfies the following relation:

$$\omega^{(1)} = \omega - \sum_{i=1}^{j} (v_i^T \omega)\, v_i + \delta_1, \qquad \|\delta_1\| = O(\boldsymbol{u}\|\omega\|) \tag{1}$$

The IMGS orthogonalisation further eliminates residual errors, as expressed by:

$$\omega^{(2)} = \omega^{(1)} - \sum_{i=1}^{j} \left(v_i^T \omega^{(1)}\right) v_i + \delta_2, \qquad \|\delta_1\| = O\left(\boldsymbol{u}\left\|\omega^{(1)}\right\|\right) \tag{2}$$

where ω denotes the unorthogonalised vector generated during the Arnoldi process; $\boldsymbol{u}$ represents the machine precision, i.e., the unit round-off error in floating-point arithmetic; v_i denotes the standard orthonormal basis vectors of the Krylov subspace; and δ_1 and δ_2 denote accumulated rounding error vectors.

After applying IMGS orthogonalization, the error is reduced to $\|\delta_1\| + \|\delta_2\| = O\left(\boldsymbol{u}^2\left\|\omega^{(1)}\right\|\right)$, effectively lowering the orthogonality error of the basis vectors from a first-order rounding error $O(\boldsymbol{u})$ to a second-order term $O(\boldsymbol{u}^2)$. This significantly improves the quality of the Krylov subspace basis. The two-stage orthogonalisation strategy effectively preserves the linear independence of the Krylov subspace basis vectors and significantly enhances the convergence stability of the algorithm, even when solving BEM matrices with extremely high condition numbers

2.2 Key techniques of the IMGS-GMRES algorithm

Consider the linear system to be solved, which takes the following form:

$$Ax = b \tag{3}$$

where $A \in R^{n\times n}$ and $b \in R^n$.

To reduce the condition number of the matrix, the original ill-conditioned linear system (Equation 3) can be transformed into an equivalent form with a lower condition number, as follows:

$$(DA)x = Db \tag{4}$$

where D is the preconditioning matrix. After preconditioning, the system becomes $\tilde{A} = DA$ and $\tilde{b} = Db$.

(1) Initialization process

Set the restart parameter m, tolerance ϵ, and initial iterate x_0.

1) Compute the initial residual:

$$\begin{cases} r_0 = \tilde{b} - \tilde{A}x_0 \\ \beta = \|r_0\| \end{cases} \tag{5}$$

2) If $\beta < \epsilon$, then return x_0 as the solution.

3) Normalise the first basis vector:

$$v_1 = \frac{r_0}{\beta} \tag{6}$$

4) Initialise matrices: define the orthonormal basis matrix as $V_k = [v_1, v_2, \ldots, v_k]$, and the upper Hessenberg matrix $\bar{H}_k$.

$$\bar{H}_k = \begin{bmatrix} h_{11} & h_{12} & \cdots & h_{1k} \\ h_{21} & h_{22} & \cdots & h_{2k} \\ \vdots & \vdots & \ddots & \vdots \\ h_{k1} & h_{k2} & \cdots & h_{kk} \\ 0 & 0 & \cdots & h_{k+1,k} \end{bmatrix} \tag{7}$$

(2) Arnoldi process with IMGS orthogonalization

For $j = 1, 2, \ldots, k$, perform the following steps:

1) Compute the matrix-vector product:

$$\beta = \widetilde{A} v_j \tag{8}$$

2) Perform first-stage MGS orthogonalisation:

$$h_{i,j}^{(1)} = {v_i}^T \omega, \qquad \omega = \omega - h_{i,j}^{(1)} v_i, \qquad i = 1, 2, \ldots, j \tag{9}$$

3) Perform second-stage IMGS orthogonalisation:

$$h_{i,j}^{(2)} = {v_i}^T \omega, \qquad \omega = \omega - h_{i,j}^{(2)} v_i, \qquad i = 1, 2, \ldots, j \tag{10}$$

4) Update the upper Hessenberg matrix elements:

$$h_{i,j} = h_{i,j}^{(1)} + h_{i,j}^{(2)} (i < j) \tag{11}$$

5) Normalise the new basis vector:

$$h_{j+1,j} = \|\omega\| \tag{12}$$

$$v_{j+1} = \frac{\omega}{h_{j+1,j}} \tag{13}$$

If $h_{j+1,j} = 0$, the Arnoldi process is terminated early.

(3) Solution of the least-squares problem

Define the unit vector $e_1 = [1, 0, \ldots, 0]^{\mathrm{T}}$, where $e_1 \in R^{k+1}$. Solve the least-squares problem: $y_k = \mathrm{argmin}\|\beta e_1 - \bar{H}_k y\|_2$. This yields the approximate solution $x_k = x_0 + V_k y_k$.

(4) Compute the residual norm:

$$\|r_m\| = \|\beta e_1 - \bar{H}_k y_k\| \tag{14}$$

if $\|r_m\| < \epsilon$, output the current solution x_k ; otherwise, perform a restart operation. When $k = m$, reset the Krylov subspace (clear V_k and $\bar{H}_k$) and restart the iteration from the current approximate solution x_k.

Although the MGS orthogonalisation process can initially ensure the orthogonality of basis vectors, its numerical accuracy is highly dependent on the degree of ill-conditioning. When the condition number of the basis matrix is large, rounding errors in floating-point arithmetic can be significantly amplified, resulting in progressive degradation of orthogonality. This error amplification effect is particularly pronounced in severely ill-conditioned problems and may lead to stagnation in residual convergence or even pseudo-convergence.

The IMGS orthogonalisation effectively addresses this bottleneck by employing a two-step orthogonalisation design. After the first orthogonalisation performs the primary projection computation, the second orthogonalisation compensates for the residual component, serving as a secondary filtering of rounding errors. This dual correction mechanism strictly confines orthogonality error within machine precision, thereby eliminating the risk of error amplification associated with increasing condition numbers.

Therefore, when solving boundary element systems with severe ill-conditioning, such as those encountered in ship hydrodynamic analysis, the IMGS orthogonalisation is capable of consistently maintaining strict orthogonality of the Krylov subspace basis vectors. This fundamentally ensures the convergence reliability of the GMRES algorithm and prevents iteration failure caused by numerical instability.

2.3 Hydrodynamic model embedded with the IMGS-GMRES algorithm

Based on linear potential flow theory, a hydrodynamic solver named FHLAN [25] has been developed. Under wave excitation, the total velocity potential Φ of the floating body can be systematically decomposed

into three key components: the incident potential Φ_{I}, the diffraction potential Φ_{D}, and the radiation potential Φ_{R} [26, 27]. Here, Φ_{I} represents the undisturbed incident wave field, characterising the direct action of the incoming wave on the floating body; Φ_{D} denotes the disturbance induced by the fixed body on the incoming wave field, reflecting the wave scattering caused by the presence of the structure; and Φ_{R}, on the other hand, arises from the oscillatory motion of the floating body and describes the radiated wave field generated by its motion in each degree of freedom.

Therefore, the total velocity potential Φ can be expressed as the sum of these three components:

$$\Phi(\boldsymbol{X},t) = \mathrm{Re}\left[\left(\Phi_{\mathrm{I}}(\boldsymbol{X}) + \Phi_{\mathrm{D}}(\boldsymbol{X}) + \Phi_{\mathrm{R}}(\boldsymbol{X})\right)e^{-i\omega_e t}\right] \tag{15}$$

where ω_e is the encounter frequency, t denotes time, and $\boldsymbol{X}$ is the position vector at a given point within the fluid domain.

The incident potential Φ_{I} is generally expressed as:

$$\Phi_{\mathrm{I}}(\boldsymbol{X}) = \frac{igA}{\omega}e^{kz}e^{-ik(x\cos\beta - y\sin\beta)} \tag{16}$$

where A is the wave amplitude of the incident wave, k is the wave number, β is the wave heading angle, and ω is the angular frequency of the wave.

When solving for the velocity potential in the external fluid domain of the floating body, it is necessary to establish a complete system of computational domain boundaries [28]. As illustrated in Figure 1, this boundary system consists of four key surface boundaries: the wetted surface of the body, which serves as the body boundary; the free surface, which represents the air-water interface; the far-field boundary, which defines the outer limit of the computational domain; and the bottom boundary, which corresponds to the bottom boundary of the fluid region.

Based on the above physical assumptions, the time-dependent velocity potential $\Phi(\boldsymbol{X},t)$ can be separated into the product of a spatial potential $\Phi(x,y,z)$ and a temporal factor $e^{-i\omega_e t}$ using the method of separation of variables. This transformation converts the original time-domain problem into a frequency-domain formulation, which satisfies the following boundary value problem:

$$\begin{cases} \nabla^2\Phi(x,y,z) = 0 & \text{entire fluid domain} \\ \dfrac{\partial\Phi}{\partial z} - k\Phi = 0 & \text{free surface} \\ \dfrac{\partial\Phi}{\partial n} = -i\omega x_j \tilde{n}_j, \quad j = 1,\cdots,7 & \text{body surface} \\ \left.\dfrac{\partial\Phi}{\partial n}\right|_{z=-H} \text{ or } \lim\limits_{z\to\infty}\nabla\Phi = 0 & \text{bottom boundary} \\ \lim\limits_{R\to\infty}\sqrt{R}\left(\dfrac{\partial\Phi}{\partial R} - ik\Phi\right) = 0 & \text{cylindrical radiation boundary} \end{cases} \tag{17}$$

where $R = \sqrt{(x^2+y^2)}$ is the radius of the far-field cylindrical surface, x_j denotes the motion amplitude in the j-th degree of freedom, and H is the water depth.

The equation of motion of the floating body in the frequency domain is given by:

$$\left[-\omega^2\left(m_{ij} + A_{ij}\right) - i\omega\left(B_{ij}\right) + C_{ij}\right]\left[\eta_j\right] = \left[F_j\right], \quad i,j = 1,\cdots,6 \tag{18}$$

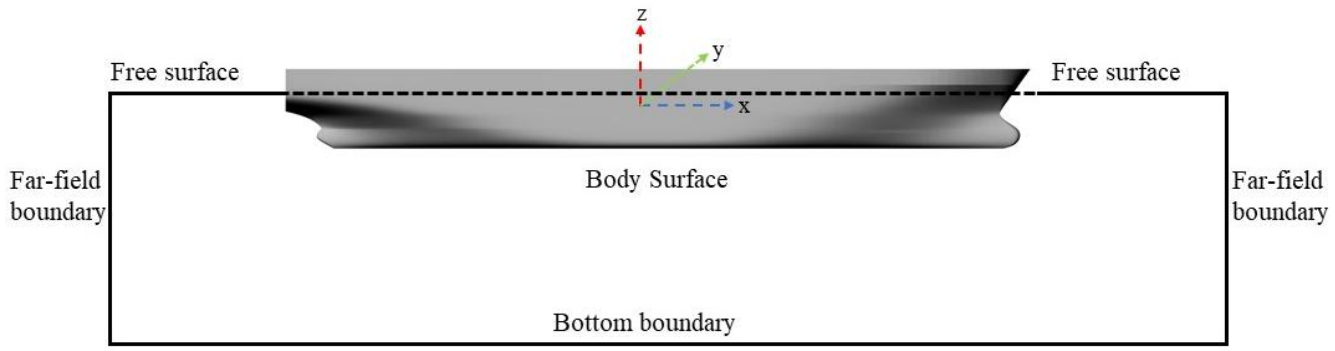

Fig. 1. Schematic diagram of the computational domain boundary surfaces

Based on BEM, the hydrodynamic analysis platform FHLAN was developed using a modular architecture, in which the entire solution procedure is divided into several functional modules. In the initialisation stage, the program first reads the input parameters, including the mass properties of the floating body, hydrostatic parameters (such as displacement and center of buoyancy), and restoring force coefficients. It then enters the geometry processing module, where the nodal coordinates and element topology of the boundary elements on the body surface are imported. Subsequently, the core computation module is activated. This module solves the free-surface Green's function based on the free-surface boundary condition and constructs and discretises the boundary integral equations, thereby forming the coefficient matrix system. The known velocity potential terms on the body boundary are then substituted into the system to complete the numerical solution of the boundary value problem. Depending on the matrix size and the degree of ill-conditioning, either a direct solver or the iterative IMGS-GMRES algorithm is selected to solve the resulting linear system and obtain the unknown velocity potential components.

Finally, based on the velocity potential on the body surface, the motion response of the vessel is solved, yielding the six degrees of freedom (6-DOF) hydrodynamic coefficients. The overall hydrodynamic solution procedure in FHLAN is illustrated in Figure 2.

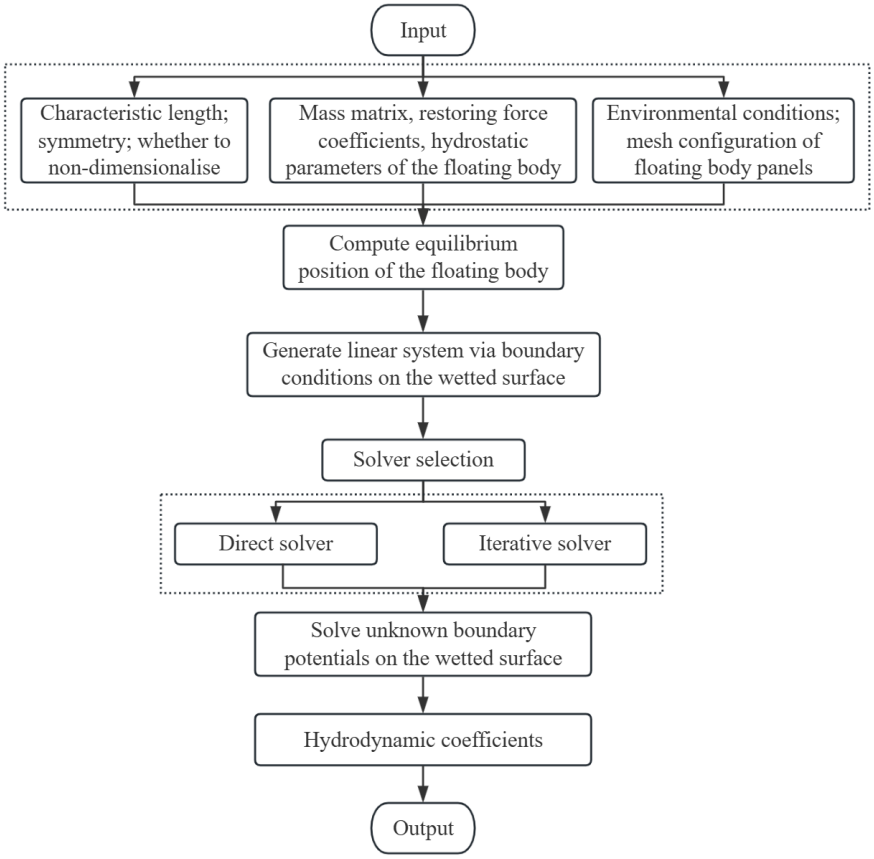

Fig. 2. Hydrodynamic solution procedure of the FHLAN numerical program

3. Numerical experiments

Based on potential flow theory, a frequency-domain hydrodynamic analysis program named FHLAN was developed using the BEM. The program integrates a direct solver employing Gaussian elimination with an iterative solver based on the IMGS-GMRES algorithm. This section presents accuracy analysis and an orthogonality error analysis is to evaluate the computational precision and numerical stability of the FHLAN. All simulations were conducted on a computer equipped with a 12th Gen Intel® Core™ i7-12650H 2.30 GHz processor and 16 GB RAM. Preliminary estimation indicates that a 8 GB RAM configuration can process approximately 32,000 meshes in FHLAN.

3.1 Accuracy analysis

The present study adopts linear potential flow in the frequency domain with a rigid-body assumption, employing radiation/diffraction decomposition and a free-surface Green function. Viscous effects, wave breaking, and scale effects are not explicitly modelled. Boundary conditions on free surface and far-field are enforced in the linearized sense; panel discretization introduces geometric approximation. In contrast, physical tank tests inherently include viscous/turbulent dissipation, 3D flow separation, model-scale Reynolds/Froude differences, sensor noise, and installation uncertainties. Consequently, experimental response curves may exhibit additional damping/phase shifts at resonance/anti-resonance.

To ensure engineering credibility under these assumptions, WADAM is used as an industry benchmark. In this section, a Liquefied Natural Gas Carrier (LNG Carrier) is selected as the research object for frequency-domain analysis. The computational accuracy of the FHLAN program, which integrates the IMGS-GMRES algorithm, is validated by comparing its hydrodynamic coefficients with those obtained using the commercial software WADAM. The principal dimensions of the LNG carrier are listed in Table 1 and illustrated in Figure 3. The frequency-domain analysis conditions are summarized in Table 2.

The comparison in Figures 4 and 5 show $R^2 \geqslant 0.957$ for added mass / damping / excitation forces, indicating that despite neglected viscous effects the present model achieves the accuracy required by ITTC guidance for frequency-domain hydrodynamics. Future work will include regular / irregular wave basin tests and viscous correction models to further tighten numerical-experimental agreement.

Table 1 Principal particulars of the LNG carrier

Item	Symbol	Unit	Value
Length overall	L_{OA}	m	140.7
Length between perpendiculars	L_{PP}	m	132.9
Breadth moulded	B	m	15
Depth moulded	D	m	21.6
Draft	T	m	10.5
Displacement	∇	t	19033

Table 2 Test case design parameters

Item	Symbol	Unit	Value
Length overall	ω	rad/s	[0.1, 8.1]
Frequency interval	$\Delta\omega$	rad/s	0.2
Water depth	H	m	Infinite
Wave heading angle	θ	°	0
Dimensionless length	L		1

(a) Geometric model

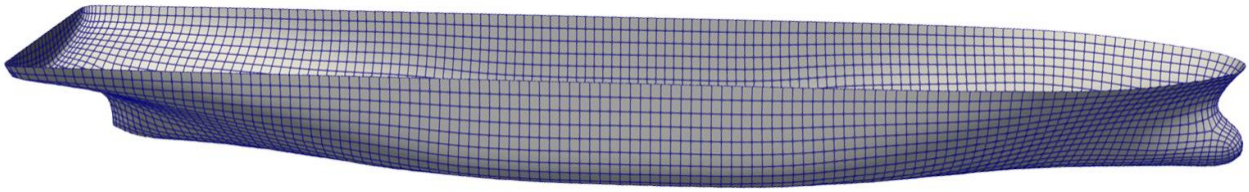

(b) Panel mesh

Fig. 3. Principal dimensions of the LNG carrier

Following the integration of the IMGS-GMRES algorithm into the FHLAN solver, the solver's hydrodynamic computational accuracy was validated against solutions obtained via Gaussian elimination.

Figure 4 compares hydrodynamic coefficients for the LNG carrier calculated by both methods, presenting key hydrodynamic parameters: added mass coefficients (A22, A66), damping coefficients (D22, D66) and wave excitation forces (F1, F3). The frequency-domain responses are exhibit consistency across the entire frequency range (0.1-8.1 rad/s). All parameters maintain consistent trends throughout the frequency range, confirming the reliability of the solution.

In both resonance regions and off-resonance zones, FHLAN's six-degree-of-freedom hydrodynamic coefficients demonstrate close agreement with WADAM benchmark solutions, and wave-excitation forces exhibit negligible deviations. This confirms that FHLAN with IMGS-GMRES achieves engineering-level accuracy, validating its suitability for practical offshore hydrodynamic analyses.

To quantify the computational accuracy of FHLAN incorproating IMGS-GMRES, hydrodynamic coefficients were benchmarked against WADAM solutions. The coefficient of determination (R^2) was employed as the error metric:

$$R^2 = 1 - \frac{SS_{res}}{SS_{bot}} \tag{19}$$

where SS_{res} is the residual sum of squares and SS_{bot} the total sum of squares. A higher R^2 value, approaching 1, indicates minimal deviation between the datasets.

Figure 5 plots R^2 alues for key hydrodynamic coefficients: added mass coefficients (A22, A66), damping coefficients (D22, D66) and wave excitation forces (F1, F3). According to the International Towing Tank Conference (ITTC) guidelines for numerical simulation accuracy, a coefficient of determination $R^2 > 0.95$ (minimum: 0.9571) is typically required. As shown in Figure 5, all six hydrodynamic parameters satisfy this criterion, indicating that the FHLAN, when integrated with the IMGS-GMRES algorithm, produces results highly consistent with those from WADAM and exhibits excellent computational reliability.

The validation results show that the IMGS-GMRES algorithm, while offering advantages in numerical stability and iteration efficiency, also meets the accuracy requirements for industrial-level hydrodynamic analysis. The current validation is based on the linear potential flow assumption and the WADAM numerical benchmark. Future research will quantify and improve the residual errors in the resonance zone through wave tank experiments and viscous corrections.

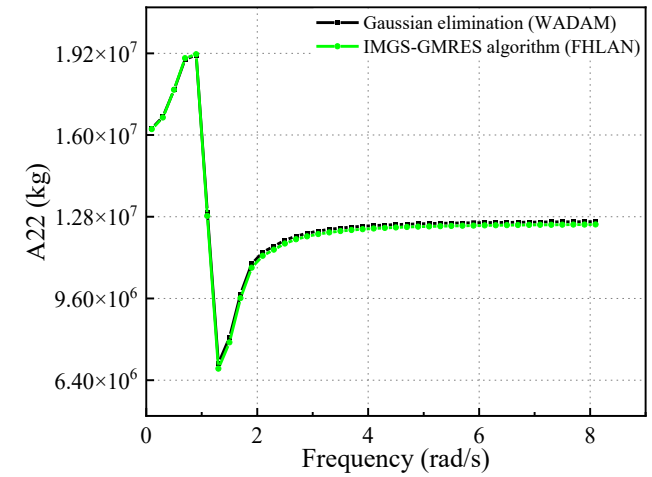

(a) Added mass A22

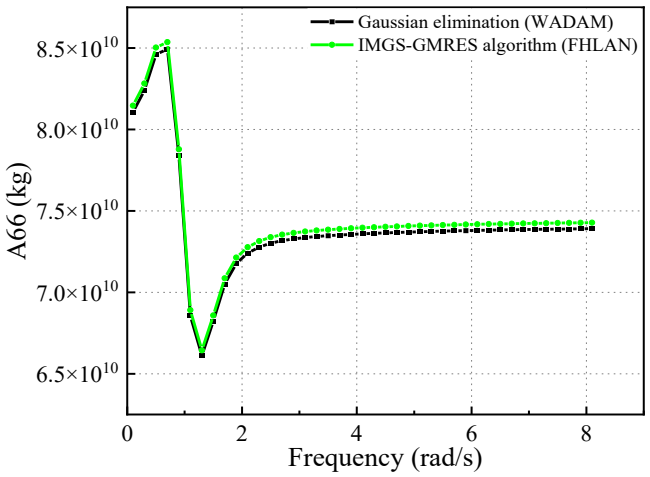

(b) Added mass A66

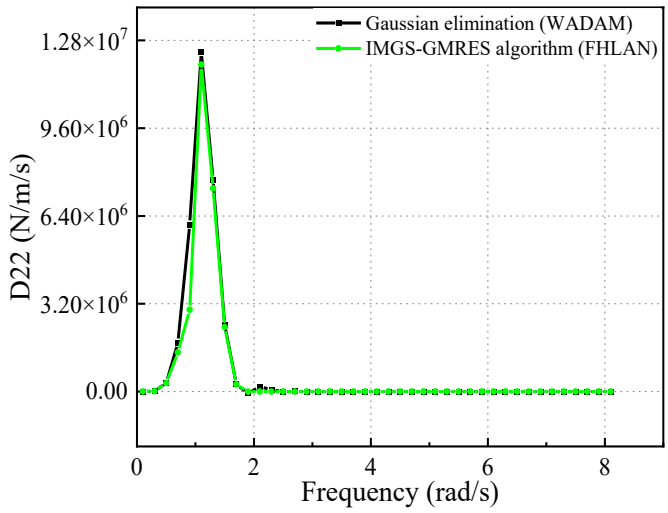

(c) Damping D22

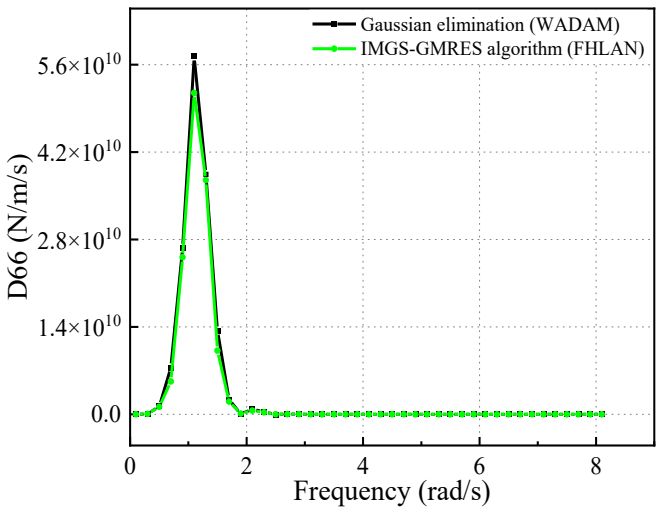

(d) Damping D66

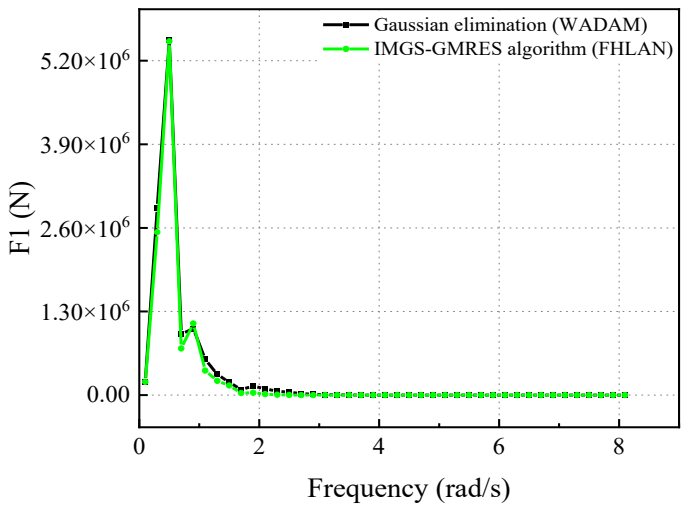

(e) Wave excitation force F1

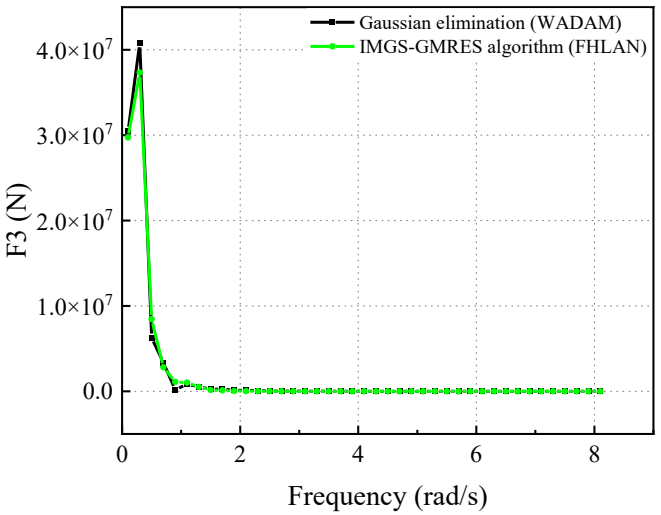

(f) Wave excitation force F3

Fig. 4. Comparison of hydrodynamic coefficients between FHLAN and WADAM

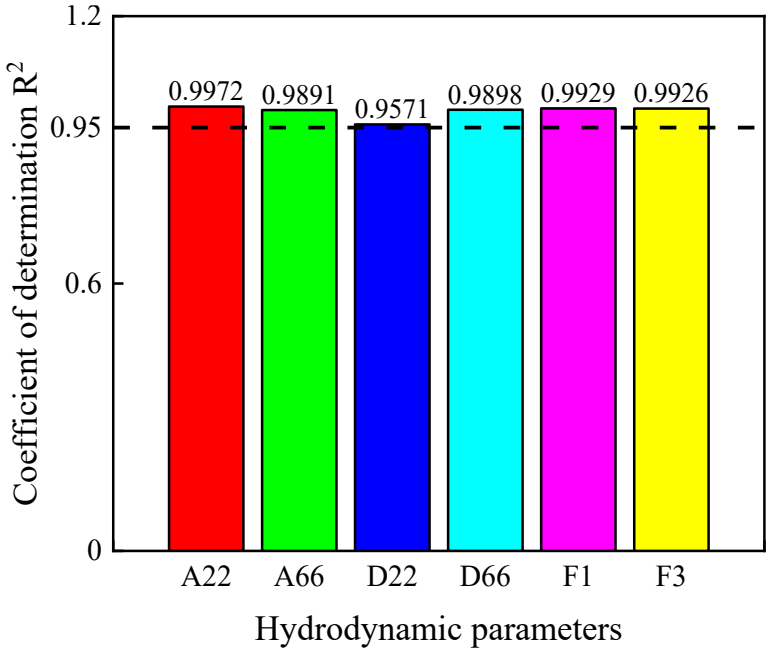

Fig. 5. Determination coefficients R^2 for hydrodynamic parameters between FHLAN and WADAM

3.2 Orthogonality error analysis

In hydrodynamic analysis, ill-conditioning in boundary element systems arises from three sources: (1) singularity in the free-surface Green's function, inducing numerical instability; (2) geometric discretisation distortion in high-curvature hull regions (panel aspect ratio > 5.0); and (3) physical field coupling effects, referring to strong nonlinear interactions between wave and structure. The combination of these effects may cause the condition number of the coefficient matrix to reach the order of 10^{14}, severely affecting numerical stability and solution accuracy.

To address the aforementioned issues, this section implements the IMGS-GMRES algorithm for numerical computations, with the problem setup detailed in Table 3.

Table 3 Frequency-domain analysis conditions

Item	Symbol	Value
Matrix dimension (mesh size)	*m*	3000
Matrix condition number	*M*	1.06×10^{22}
Convergence tolerance	*tol*	1.0×10^{-10}
Maximum iterations	*maxit*	1000

This section compares the traditional MGS and proposed IMGS-GMRES algorithms in terms of orthogonality error when solving ill-conditioned linear systems. Figure 6 illustrates the evolution of orthogonality error with iteration steps for both methods, with corresponding performance indicators summarized in Table 4.

Table 4 Comparison of results

Item	MGS	IMGS
Number of iterations	498	275
Final residual	1.02×10^{-6}	1.02×10^{-6}
Maximum orthogonalisation error	7.43×10^{-12}	4.11×10^{-16}
Relative error	1.0×10^{-9}	1.0×10^{-11}

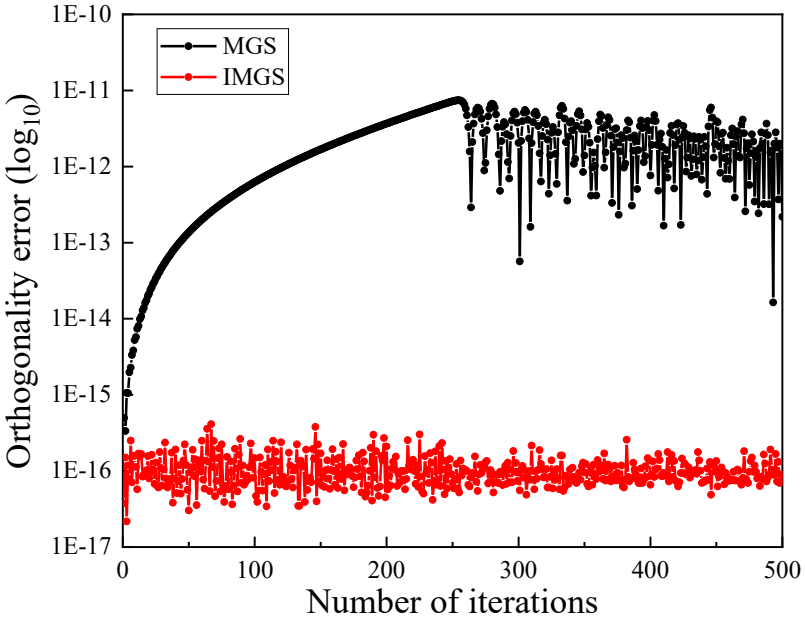

Fig. 6. Comparison of orthogonality errors

As shown in Figure 6, the MGS method exhibits rapid accumulation of orthogonality error in the initial phase. With increasing iteration steps, the error grows significantly and markedly fluctuate after approximately 220 steps, reaching a maximum orthogonality error of 7.43×10^{-12}. This indicates the method's poor capability to preserve orthogonality when dealing with high-condition-number systems. In contrast, the IMGS method demonstrates excellent numerical stability throughout all iterations, with orthogonality error consistently confined within machine precision (approximately 4.11×10^{-16}) without noticeable fluctuations. This highlights the effectiveness of its dual orthogonalisation correction mechanism in curbing cumulative errors.

Table 4 shows that at an identical residual level (1.02×10^{-6}), the IMGS algorithm requires only 275 iterations - approximately 44.8 % fewer than the MGS method's 498 iterations. Additionally, IMGS achieves a relative solution error of 1.0×10^{-11}, two orders of magnitude below the MGS result (1.0×10^{-9}), demonstrationg its substantially enhanced precision control.

Consequently, the IMGS-GMRES algorithm surpasses traditional methods in both iteration efficiency orthogonality preservation, and numerical accuracy, rendering it ideally suited for solving high-dimensional, severely ill-conditioned boundary element discretised systems.

Theoretical analysis of orthogonality error is essential for evaluating the numerical stability of the IMGS orthogonalisation process. For the basis matrix of the Krylov subspace:

$$V_k = [v_1, v_2, \ldots, v_k] \tag{20}$$

It's ideal orthogonality condition should satisfy:

$$V_k^T V_k = I_k \tag{21}$$

here, I_k denotes the identity matrix. However, in practical computations, floating-point rounding errors cause the matrix V_k to deviate from its ideal orthogonal state. Therefore, the orthogonality error matrix can be defined as:

$$E_k = V_k^T V_k - I_k \tag{22}$$

Accordingly, the metric for quantifying orthogonality error is defined as the maximum element-wise error, denoted by $\|E_k\|_\infty$, which is specifically given by:

$$\|E_k\|_\infty = \max_{i \neq j} \left| v_i^T v_j \right| \tag{23}$$

Figure 6 compares orthogonality error of MGS and IMGS orthogonalisation methods under the frequency-domain analysis conditions listed in Table 3. The MGS method exhibits oscillatory behaviour from approximately iteration 220 onwards. This oscillation stems primarily from the severely ill-conditioned linear systems in BEM discretisation.

In contrast, the IMGS orthogonalisation method consistently maintains the orthogonality error in a steady state at approximately 1.0×10^{-16}. The GMRES iterative algorithm with IMGS orthogonalisation demonstrates significant advantages in high-condition-number scenarios. Compared to the MGS method, the IMGS approach reduces the number of iterations by 44.78 % (from 498 to 275 steps), decreases orthogonality error by four orders of magnitude (from 7.43×10^{-12} to 4.11×10^{-16}), and achieves higher solution accuracy, with relative error reduced from 1.0×10^{-9} to 1.0×10^{-11}.

Therefore, the IMGS orthogonalisation method is particularly ideally suited to solving ill-conditioned systems stemming from BEM discretisation in hydrodynamic analysis.

The convergence rate has a substantial impact on computational efficiency, and it is therefore essential to examine the convergence behaviour of the IMGS-GMRES algorithm in detail. Table 5 compares iteration counts for the MGS and IMGS algorithms under different tolerance levels, matrix dimension being fixed at 3000.

Table 5 Iteration count comparison under different tolerance levels

Tolerance	Number of iterations		Reduction ratio of iterations (%)
	MGS	IMGS	
10^{-4}	32	26	18.75
10^{-6}	89	58	34.83
10^{-8}	214	128	40.19
10^{-10}	498	275	44.78
10^{-12}	Not converged	529	-

The results indicate that, under equivalent tolerance conditions, the number of iterations required by the IMGS algorithm consistently decreases as the stricter convergence criteria. In contrast, under a stringent tolerance of 10-12, the MGS method fails to converge due to the degradation of orthogonality, while the IMGS algorithm successfully converges within 529 iterations.

By employing a dual orthogonalisation correction, the IMGS method effectively suppresses the accumulation of orthogonality error and rigorously confines them within machine precision. This eliminates the risk of error amplification in highly ill-conditioned problems, thereby ensuring residual stability and a monotonic convergence profile.

In engineering applications involving ill-conditioned boundary element equations such as hydrodynamic analyses of ships the proposed method significantly reduces computational cost under moderate to high accuracy requirements. Furthermore, it demonstrates irreplaceable reliability under extremely strict precision demands, indicating a broad potential for practical implementation.

3.3 Analysis of different mesh densities

In hydrodynamic analysis, surface mesh element count critically influences computational result accuracy and stability [29, 30]. Within BEM, the mesh density directly determines the dimensionality of the resulting linear system. In IMGS-GMRES algorithm, mesh density corresponds directly to the dimension of the system matrix.

This section benchmarks of the algorithm's performance under varying mesh densities, in order to systematically assess the overall capability of the IMGS-GMRES algorithm in solving high-dimensional ill-conditioned problems. The LNG carrier model shown in Figure 3 is adopted as the benchmark case, and the specific simulation conditions are listed in Table 6.

Table 6 Simulation conditions for mesh density analysis

Item	Symbol	Value
Number of mesh elements	N	[1000, 31000]
Grid increment step	ΔN	2000
Convergence tolerance	*tol*	1.0×10^{-10}
Maximum number of iterations	*maxit*	1000

Figure 7 presents a comparison of the iteration counts between the MGS and IMGS methods under a fixed convergence tolerance of 1.0×10^{-10} as the number of mesh panels increases. Overall, the IMGS method exhibits a significantly lower iteration count compared to MGS, and this reduction becomes more pronounced as the mesh density increases. This trend highlights the superior scalability and robustness of the IMGS approach in handling large-scale problems.

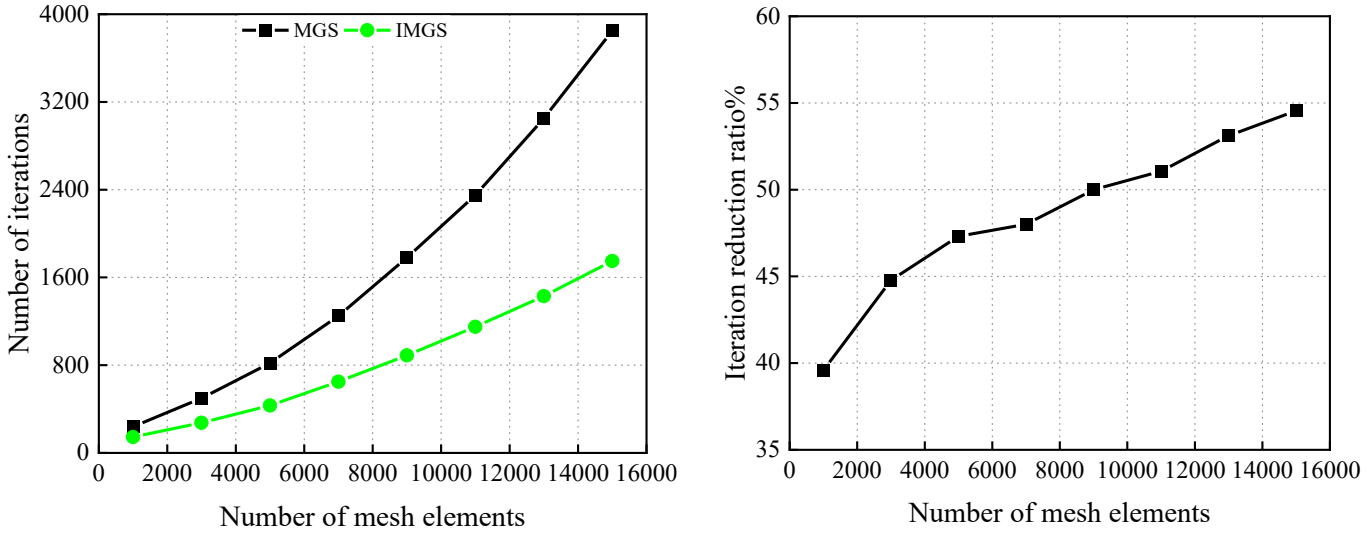

(a) Comparison of iteration counts between MGS and IMGS methods

(b) Percentage reduction in iteration counts achieved by IMGS relative to MGS

Fig. 7. Iteration performance under varying mesh densities

Figure 8 illustrates the comparison of orthogonality error under different mesh densities. As the matrix dimension increases, the orthogonality error associated with the MGS method exhibits exponential accumulation due to the magnification effect of high condition numbers. This leads to residual stagnation and even divergence in the later stages of iteration. In contrast, the IMGS method, through its dual orthogonalisation correction mechanism, effectively confines the error within the machine precision range of 1.0×10^{-16} to 1.0×10^{-15}, thereby eliminating the error propagation chain.

The numerical experiments also compared the computational time between the direct solver based on Gaussian elimination and the iterative solver using the IMGS-GMRES algorithm, as shown in Figure 9. It can be observed that when the mesh density is relatively low, the iterative method does not exhibit a clear advantage in computation speed over the direct method. However, as the number of mesh elements increases, the performance of the iterative solver improves significantly. The larger the problem size, the more pronounced the speed-up becomes. This demonstrates that the IMGS-GMRES algorithm is particularly well-suited for large-scale hydrodynamic problems.

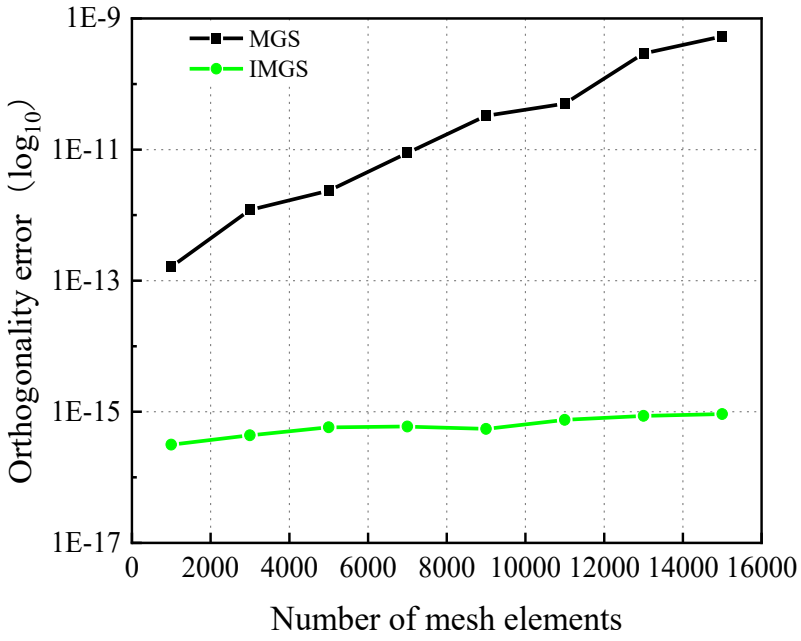

Fig. 8. Comparison of orthogonality error under different grid numbers

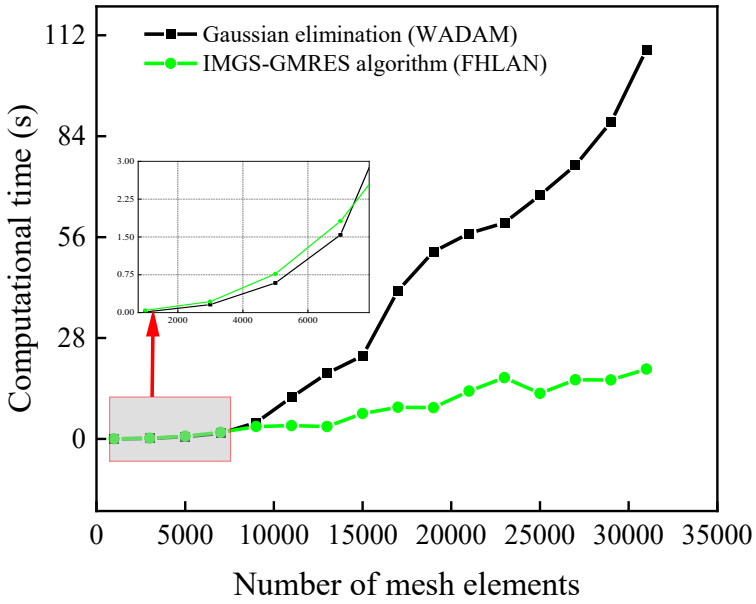

Fig. 9. Comparison of solving time between Gaussian elimination and IMGS-GMRES algorithms under different grid numbers

4. Conclusion

To address the ill-conditioning problems arising in large-scale hydrodynamic simulations caused by Green's function singularities, geometric discretisation distortion, and strong coupling of physical fields a novel IMGS-GMRES algorithm is proposed in this study for efficiently solving such large linear systems. The main conclusions are as follows:

(1) The IMGS-GMRES algorithm ensures high accuracy in hydrodynamic computations through a rigorous dual orthogonalisation error control.

By employing a dual orthogonalisation scheme, it effectively compensates for projection residuals left by initial orthogonalisation. This guarantees a strictly monotonic residual convergence even when solving BEM matrices with high dimensionality and extreme condition numbers. Unlike the traditional MGS method, which often suffers from residual oscillations due to cumulative numerical errors, the proposed approach

maintains numerical stability throughout. Consequently, the algorithm demonstrates marked advantages in applications requiring high precision and robustness, such as ship hydrodynamic analysis, and represents a reliable core solver for ill-conditioned systems.

(2) The IMGS-GMRES algorithm significantly enhances computational efficiency while preserving accuracy.

By applying rigorous orthogonality correction to the basis vectors, it markedly reduces the frequency of Krylov subspace reconstructions and avoids redundant iterations caused by degraded orthogonality. Through a two-pass Gram-Schmidt procedure, the algorithm confines orthogonality error to the level of machine precision, effectively eliminating the risk of error amplification in high-dimensional, ill-conditioned systems. In large-scale problems-particularly when the number of panels (i.e., the matrix dimension) exceeds 8000 the performance advantage of the IMGS-GMRES algorithm becomes increasingly prominent. For instance, with 31,000 mesh elements, it achieves an 82 % reduction in computation time compared to conventional direct solvers, demonstrating its superior scalability for large-scale hydrodynamic simulations.

(3) The IMGS-GMRES algorithm is particularly well-suited for large-scale hydrodynamic problems characterized by high dimensionality, severe ill-conditioning, and stringent accuracy requirements.

When the discretized boundary element matrices exceed 8000 degrees of freedom and the condition number surges beyond 10^8 due to geometric singularities or strong physical coupling effects, the IMGS algorithm ensures stable convergence through its dual orthogonalisation correction scheme. Moreover, in complex scenarios involving multi-body interactions or high-frequency excitations, the algorithm effectively suppresses orthogonality degradation of the Krylov subspace basis vectors, thereby eliminating spurious modal contamination and ensuring the accuracy of eigenvalue extraction in frequency-domain analysis.

ACKNOWLEDGEMENT

This research was funded by the National Natural Science Foundation of China (Grant No.52271293), Key R&D Plan Projects in Zhejiang Province (Grant No.2019C02087).

REFERENCES

[1] Ozdemir, Y. H., Cosgun, T., Barlas, B., 2021. Wave field generated by finite-span hydrofoils operating beneath a free surface. *Brodogradnja*, 72(1), 145-167. https://dx.doi.org/10.21278/brod72108

[2] Bai, W., Zhang, W., Cao, L., Liu, Q., 2023. Adaptive control for multi-agent systems with actuator fault via reinforcement learning and its application on multi-unmanned surface vehicle. *Ocean Engineering*, 280, 114545. https://doi.org/10.1016/j.oceaneng.2023.114545

[3] Liu, L., Zhang, B., Zhang, H., Tang, H., Wang, W., 2023. Hydrodynamic performance optimisation of marine propellers based on fluid-structure coupling. *Brodogradnja*, 74(3), 145-164. https://dx.doi.org/10.21278/brod74308

[4] Zheng, S. W, Kou, J., Zhang, W., 2025. Hybrid-precision GMRES acceleration algorithm for large-scale sparse matrices in fluid dynamics simulation. *Applied Mathematics and Mechanics*, 46(1), 40-54.

[5] Carr, A. K., de Sturler, E., Embree, M., 2023. Analysis of GMRES for low-rank and small-norm perturbations of the identity matrix. *PAMM-Proceedings in Applied Mathematics and Mechanics*, 22(1), e202200267. https://doi.org/10.1002/pamm.202200267

[6] Sun, J., Zheng, X., Liu, Y., Yao, Z., 2021. Some investigations on convergence of GMRES in solving BEM equations for slender beam structures. *Engineering Analysis with Boundary Elements*, 126, 128-135. https://doi.org/10.1016/j.enganabound.2021.02.009

[7] Cheng, Y., Ji, C., Zhai, G., Fan, T., 2017. Investigation of hydroelastic behaviour of a pontoon-type VLFS during unsteady external loads in wave condition using a hybrid finite element-boundary element (FE-BE) method. *Brodogradnja*, 68(4), 23-41. https://dx.doi.org/10.21278/brod68402

[8] Hess, J. L., Smith, A. M. O., 1964. Calculation of potential flow about arbitrary bodies. *Progress in Aerospace Sciences*, 8, 1-138. https://doi.org/10.1016/0376-0421(67)90003-6

[9] Saad, Y., Schultz, M. H., 1986. GMRES: A generalised minimal residual algorithm for solving nonsymmetric linear systems. *SIAM Journal on Scientific and Statistical Computing*, 7(3), 856-869. https://doi.org/10.1137/0907058

[10] Liu, H., 2022. Research on low-synchronisation Krylov subspace algorithms. *Master Thesis*, Beijing University of Posts and Telecommunications, Beijing, China.

[11] Zounon, M., Higham N., J, Lucas, C., Tisseur, F. 2022. Performance impact of precision reduction in sparse linear sys tems solvers. *PeerJ. Computer science,* 8, e778. http://doi.org/10.7717/peerj-cs.778

[12] Muzhinji, K., 2023. Optimal block preconditioner for an efficient numerical solution of the elliptic optimal control problems using GMRES solver. *International Journal of Numerical Analysis and Modeling,* 20(1), 47-66. https://doi.org/10.4208/ijnam2023-1003

[13] Göbel, F., Grützmacher, T., Ribizel, T., Anzt, H., 2021. Mixed precision incomplete and factorised sparse approximate inverse preconditioning on GPUs. In: Sousa, L., et al. (eds.), *Euro-Par 2021: Parallel Processing, Lecture Notes in Computer Science (LNCS)*, Vol. 12820, pp. 550-564. Springer, Cham. https://doi.org/10.1007/978-3-030-85665-6_34

[14] Zhang, X. F., Xiao, M. L., He, Z. H., 2025. Orthogonal block Kaczmarz inner-iteration preconditioned flexible GMRES method for large-scale linear systems. *Applied Mathematics Letters*, 166, 109529. https://doi.org/10.1016/j.aml.2025.109529

[15] Carson, E., Higham, N. J., 2020. Accelerating the solution of linear systems by iterative refinement in three precisions. *SIAM Journal on Scientific Computing*, 40(2): A817-A847. https://doi.org/10.1137/17M1140819

[16] Gragg, W. B., Kaufman, L., Stewart, G. W., 2022. Block Gram-Schmidt algorithms and their stability properties. *Linear Algebra and its Applications*, 640, 25-44. https://doi.org/10.1016/j.laa.2021.12.017

[17] Zhou, S. W., Yang, A. L., Wu, Y. J., 2017. Two modified block-triangular splitting preconditioners for generalised saddle-point problems. *Computers & Mathematics with Applications*, 74(6), 1176-1197. https://doi.org/10.1016/j.camwa.2017.06.004

[18] Simoncini, V., Gallopoulos, E., 1995. An iterative method for nonsymmetric systems with multiple right-hand sides. *SIAM Journal on Scientific Computing*, 16(4), 917-933. https://doi.org/10.1137/0916053

[19] Dai, Y. Z., Song, J. Z., Ren, H. L., Li, H., 2003. Application of GMRES to the hydroelastic analysis of large offshore structures. *The Ocean Engineering*, 21(4), 15-22. https://doi.org/10.16483/j.issn.1005-9865.2003.04.003

[20] Bai, W., Chen, D., Zhao, B., D'Ariano, A., 2025. Reinforcement learning control for a class of discrete-time non-strict feedback multi-agent systems and application to multi-marine vehicles. *IEEE Transactions on Intelligent Vehicles*, 10(5), 3613-3625. https://doi.org/10.1109/TIV.2024.3458894

[21] Ucar, M., Hmidi, M., Uzunoglu, E., Oguz, E., 2025. Effect of panel method codes in estimating the time-domain responses of floating wind turbines. *Brodogradnja*, 76(2), 76203. http://dx.doi.org/10.21278/brod76203.

[22] Ghassabzadeh, M., Ghassemi, H., Saryazdi, M. G., 2013. Determination of hydrodynamics characteristics of marine propeller using hydro-elastic analysis. *Brodogradnja*, 64(1), 40-45.

[23] Zabala, I., Henriques, J.C.C., Kelly, T.E., Ricci, P.P., Blanco, J.M., 2024. Post-processing techniques to improve the results of hydrodynamic Boundary Element Method solvers. *Ocean Engineering*, 295, 116913. https://doi.org/10.1016/j.oceaneng.2024.116913

[24] Zhang, H., Zhang, H., You, W. J., Zheng, H. Y., 2021. A method of inhibiting pathogeny for ill-conditioned problems of the finite element discrete systems of 2D boundary value problems. *Advances in Applied Mathematics*, 10(12), 4162-4171. https://doi.org/10.12677/aam.2021.1012442

[25] Wang, W., Xie, Y., Zhang, J., Li, G., 2024. Design and Optimization of Layout and Dimensions of the M4 Wave Energy Converter System Under Regular and Irregular Waves. *ASME 2024 43rd International Conference on Ocean, Offshore and Arctic Engineering*, 9-14 June, Singapore.

[26] Qiu, W., Wang, Z., Jiang, M., Lin, L., 2022. Prediction approach for wave forces on large-scale offshore structures under linear wave action. *Ocean Engineering*, 257, 111694. https://doi.org/10.1016/j.oceaneng.2022.111694

[27] Li, H., Hao, L., Ren, H., Tian, B., 2017. The application of meshless cylinder control surface in Rankine-Kelvin hybrid method. *Brodogradnja*, 67(3), 87-113. https://dx.doi.org/10.21278/brod67306

[28] Nguyen, H.P., Wang, C.M., 2022. Finite element-multi-domain boundary element method for hydroelastic analysis of large floating pontoons with perforated plates. *Ocean Engineering*, 246, 110659. https://doi.org/10.1016/j.oceaneng.2022.110659

[29] Liu, J., Wu, S., Yue, X., Yue, Q., 2024. Hydrodynamic shape optimization of an autonomous and remotely-operated vehicle via a multi-surrogate model. *Brodogradnja*, 75(3), 75301. http://dx.doi.org/10.21278/brod75301

[30] Wei, Y., Zhang, J., Liu, K., Pan, J., Zhang, L., Chen, W., Zhang, Q., 2025. Numerical study of the influence of hydrofoil hydrodynamic performance considering near-free surface. *Brodogradnja*, 76(1), 76108. http://dx.doi.org/10.21278/brod76108